

# Morphological and structural variations of Nickel-Titanium endodontic instruments subjected to instrumentation loads: in vitro study

## Variaciones morfológicas y estructurales de instrumentos endodónticos de Níquel-Titanio sometidos a cargas de instrumentación: estudio in vitro

Yenny Marcela Orozco-Ocampo <sup>1a</sup>, César Augusto Álvarez-Vargas <sup>1b</sup>, Francly Nelly Jiménez-García <sup>1c, 2</sup>, Daniel Escobar-Rincón <sup>3</sup>, Paola Ximena Jaramillo-Gil <sup>1d</sup>

<sup>1</sup> Diseño Mecánico y Desarrollo Industrial – Archytas, Física y Matemáticas con Énfasis en la Formación de Ingenieros, 1 Universidad Autónoma de Manizales, Colombia. Orcid: 0000-0003-1907-6518 <sup>a</sup>, 0000-0002-4417-3865 <sup>b</sup>, 0000-0003-1546-8426 <sup>c</sup>, 0000-0001-5310-3626 <sup>d</sup>. Emails: [yorozco@autonoma.edu.co](mailto:yorozco@autonoma.edu.co) <sup>a</sup>, [dekinov@autonoma.edu.co](mailto:dekinov@autonoma.edu.co) <sup>b</sup>, [francy@autonoma.edu.co](mailto:francy@autonoma.edu.co) <sup>c</sup>, [paolax.jaramillo@autonoma.edu.co](mailto:paolax.jaramillo@autonoma.edu.co) <sup>d</sup>

<sup>2</sup> Aplicaciones y Enseñanza de las Ciencias Exactas y Naturales, Universidad Nacional de Colombia, Colombia.

<sup>3</sup> Magnetobiología, Universidad de Caldas, Colombia. Orcid: 0000-0003-4600-5117. Emails: [daniel.escobar@ucaldas.edu.co](mailto:daniel.escobar@ucaldas.edu.co)


Received: 30 May 2024. Accepted: 4 October 2024. Final version: 15 November 2024.

### Abstract

To identify morphological and structural variations in WaveOne Gold Primary® related to artificial canal instrumentation, experiments were conducted on artificial canals fabricated from Diallyl-Phthalate to identify morphological and structural variations in WaveOne-Gold-Primary (n=10) endodontic instruments. The canals were immersed in water at 38° C ± 1°C and irrigated with NaClO-5%. The instruments were examined using optical microscopy to perform Cauchy strain measurements. Lattice parameters, microstrains, and texture were determined using X-ray diffraction. Scanning electron microscopy was employed to identify shear bands and fracture characteristics. Statistical analysis was performed using analysis of variance and Bonferroni tests. Untwisting and elongation were pronounced at approximately 54 pecks; fracture occurred at 62 pecks. Mathematical models were proposed to correlate strains and texture with the number of pecks. Substantial plastic deformations caused by the torsion-adhesion mechanism and associated with ductile fracture were observed, and grain domain alterations were identified. The difference between the sample's relative intensities in X-ray diffraction demonstrated texture changes between 0 and 20 pecks and a subsequent change after 62 pecks.

**Keywords:** Endodontic instrument; NiTi alloy; Optical microscopy; XRD; SEM; Artificial root canal; Cauchy strain; Bézier curves; Fracture; WaveOne Gold Primary.

ISSN Online: 2145 - 8456

This work is licensed under a Creative Commons Attribution-NoDerivatives 4.0 License.  CC BY-ND 4.0  
How to cite: Y. M. Orozco-Ocampo, C. A. Álvarez-Vargas, F. N. Jiménez-García, D. Escobar-Rincón, P. X. Jaramillo-Gil, "Morphological and structural variations of Nickel-Titanium endodontic instruments subjected to instrumentation loads: in vitro study," *Rev. UIS Ing.*, vol. 23, no. 4, pp. 31-44, 2024, doi: <https://doi.org/10.18273/revuin.v23n4-2024003>

## Resumen

Para identificar variaciones estructurales y morfológicas de las limas endodónticas WOG Primary a medida que instrumentaban canales artificiales, se realizaron experimentos en canales artificiales fabricados con Dialil ftalato para identificar variaciones morfológicas y estructurales en instrumentos endodónticos WaveOne-Gold-Primary (n=10). Los canales se sumergieron en agua a  $38^{\circ}\text{C} \pm 1^{\circ}\text{C}$  y se irrigaron con NaClO-5%. Los instrumentos se inspeccionaron mediante microscopía óptica para medir la deformación unitaria de Cauchy. Los parámetros de red, la microdeformación y la textura se obtuvieron mediante difracción de rayos X. Se utilizó microscopía electrónica de barrido para identificar bandas de deslizamiento y caracterizar la fractura. Se utilizaron análisis de varianza y pruebas de Bonferroni para los datos. El desentorchamiento y el alargamiento fueron pronunciados cerca de 54 picoteos; a 62 picoteos se produjo la fractura. Se propusieron modelos matemáticos para relacionar la deformación unitaria y la textura con el número de picoteos. Se observaron grandes deformaciones plásticas relacionadas con fractura dúctil, causada por un mecanismo de torsión-adhesión. La diferencia entre las intensidades relativas en difracción de Rayos-X de la muestra evidenció cambios de textura entre 0 y 20 picoteos y un nuevo cambio después de 62 picoteos.

**Palabras clave:** Instrumento endodóntico; Aleación NiTi; Microscopía óptica; XRD; SEM; Canal radicular artificial; Deformación de Cauchy; Curvas Bézier; Fractura; WaveOne Gold Primary.

## 1. Introduction

The fracture of endodontic instruments is attributed to the combined effects of bending and torsional loads. Furthermore, the pecking motions (corresponding to the frequency of instrument insertion and withdrawal from the canal) during canal instrumentation result in increased strains [1]. The complex anatomy of the root canal system, characterized by curvatures and variations, subjects these instruments to bending and torsional forces [2]. The natural curvatures of the canal induce bending, while torsional stress occurs when the instrument tip becomes engaged within the canal while rotation continues.

Endodontic instruments composed of nickel-titanium (NiTi) exhibit advantageous shape memory and super-elastic properties, enabling them to recover from substantial strain (up to 10%) [3], [4]. However, these ostensibly resilient instruments are susceptible to unanticipated fractures during root canal procedures. Fractures predominantly occur at the point of maximum canal curvature, with an elevated risk in canals characterized by significant curvature and complex morphology [5].

According to previous research, fatigue is a significant factor in the failure of an instrument, typically reported within low cycles (less than  $10^4$ ) [6], which indicates that strain measurement on the instrument is critical in predicting breakage. Furthermore, the reduced size of these instruments impedes visual assessment of the point of weakness prior to fracture occurrence [7]. The instrument's life condition can subsequently be estimated by monitoring superficial deformations and recording the variations in the endodontic instrument's geometry and surface [8], [9]. These alterations were documented and

measured utilizing optical microscopy and scanning electron microscopy (SEM).

In vitro studies predominantly employ polymers, metals, or alternative materials to simulate radicular canals. These investigations frequently quantify the time to fracture in relation to revolutions and calculate the number of cycles to failure, referred to as the number of cycles to fracture (NCF) [10], [11]. The rotation of the instrument within the radicular canal corresponds to a cycle of combined bending and torsional loads. These forces induce alterations in the instrument material that may result in fracture [12], which can be identified through X-ray diffraction analysis (XRD).

This investigation aimed to identify the morphological and structural variations in WaveOne Gold Primary® (WOG) instruments and elucidate their relationship to canal instrumentation. Additionally, it sought to establish correlations between instrument surface variations, lattice parameters, texture, and number of pecks. Although this study was conducted on endodontic training canals fabricated from Diallyl Phthalate (Poly), the results are not generalizable to the behavior observed in dentine. The data obtained from the morphological and structural characterization of the instruments provided a valuable foundation for future studies on alternative canal materials and dentin.

## 2. Materials and methods

The sample size utilized in this study was determined through a pilot experiment employing a power test (error type II  $\beta=0.05$ ), resulting in a minimum of five replications per factor (number of pecks). The experimental unit for the study was WaveOne Gold Primary®, which exhibits a reciprocating motion,

parallelogram cross-section, and taper varying between 3% and 7% [13]. Ten (n=10) WOG Primary instruments and 30 canals fabricated from Poly, featuring J-type canals with a straight length of 12 mm, curvature radius, and angle of 5 mm and 30°, respectively, were employed for the tests. The artificial canals were immersed in heated water (38 ± 1°C) utilizing an experimental setup that simulated the oral cavity temperature, as illustrated in Figure 1.

For artificial canal irrigation, NaClO-5% was utilized, and the glide path was established using a ProGlider® instrument. Canal instrumentation was completed using the WOG instrument. An expert conducted all endodontic procedures. After every three pecking motions, the instruments were cleaned with deionized water and examined using optical microscopy. Considering that an endodontic training canal can be instrumented with approximately 16 pecking motions, approximately five canals were utilized until the WOG experienced failure through separation. An X-Smart Plus Dentsply Sirona motor (A1032) operating at 300 r/min and 2.5 N·cm executed the reciprocating movement.

## 2.1. Optical microscopy

Optical microscopy was conducted at intervals of three pecks. A two-component system was employed to acquire images at 400x magnification. This system comprised a portable optical microscope (Proscope HR2 Advanced Lab) and an XYZ-stage platform with calibrated displacement in the three axes utilizing a micrometric screw. An R-type sample holder was additionally positioned on the platform to provide one degree of freedom (rotation along the endodontic

instrument's longitudinal axis). This system was utilized for surface inspection and to capture images of the WOG instrument.

To quantify the surface strains of the endodontic instruments or machining line deformations, Bézier curves (five control points) were utilized. The measurements were conducted on the WOG images obtained via optical microscopy, employing the software ImageJ® [14] at 400x magnification and 1280 × 1024-pixel resolution.

The strains were quantified using the Lagrangian method, which records geometric alterations in the machined surface paths of the endodontic instrument. The conversion between pixels and millimeters was established using a calibration grid with a known length of 100 µm. Through the calibration grid, it was determined that 179 pixels corresponded to 0.1 mm for the utilized magnification and pixel resolution.

The Cauchy strain ( $\epsilon_c$ ) was calculated using Equation 1 [6]. Five randomly selected images of the WOG Primary were utilized to perform strain measurements at varying numbers of pecks.

$$\epsilon_c = \frac{L_f - L_0}{L_0}, \quad (1)$$

The line designated as number one corresponds to the base measurement distance of 0.100 mm, to which the measured error was applied. Lines three through seven are Bézier lines ( $L_f$ ), while line two represents the initial length of the machining mark ( $L_0$ ).

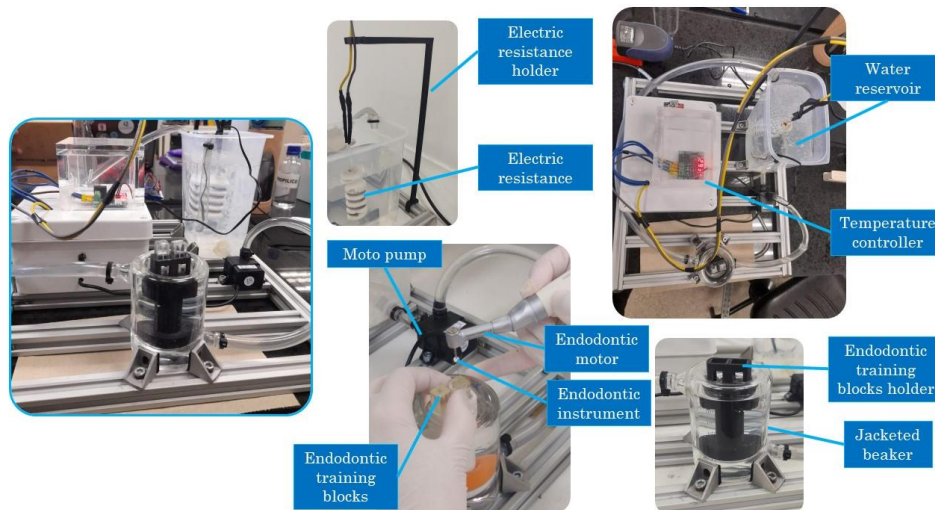


Figure 1. Setup for simulating oral cavity temperature.

The measurement protocol for the machining marks is illustrated in Figure 2.

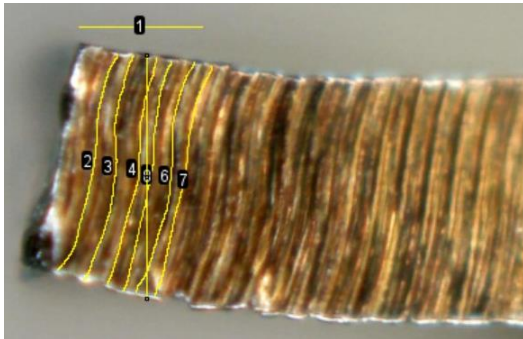


Figure 2. Machining path marks for strain measuring.

## 2.2. Scanning electron microscopy

A TESCAN VEGA 4 instrument was utilized to analyze the surface morphology of the fractured endodontic instruments. The WOGs were mounted on an aluminum stub using conductive carbon tapes and examined under high- and low-vacuum conditions (acceleration voltage of 30 kV). Images at magnifications ranging from 130x to 4600x were obtained from the fracture surfaces.

## 2.3. X-ray diffraction

X-ray diffraction (XRD) patterns of the WOG instruments were obtained utilizing a Bruker D8 Advance system in a Bragg-Brentano configuration. A radiation wavelength of 1.5406, corresponding to a copper tube, was generated by applying 40 mA and 40 kV to the direct current power source of the X-ray generation system. The step was established at  $0.02^\circ$  considering the limited measured portion of the specimen. The time was set to 60 s per step to enhance the diffraction signal statistics of the detector. Scanning from  $10^\circ$  to  $110^\circ$  was conducted to observe the diffraction peaks of the NiTi phase or oxides in the diffraction pattern.

Based on this result, the diffraction angle ( $2\theta$ ) of the endodontic instrument, was established between  $41^\circ$  and  $44^\circ$ . The aperture slits for the divergent and anti-divergent X-ray beams were adjusted to 0.7 mm to minimize background noise without compromising the diffraction peak intensity. Subsequently, a Nickel filter was employed to eliminate  $K_\beta$  radiation lines.

## 2.4. Statistical analysis

One-way analysis of variance (ANOVA) with 95% confidence interval was employed to assess the statistical

significance of the Cauchy strains of the vertical-machine surface paths of the endodontic instrument and the number of pecks. The Kruskal-Wallis and Levene tests were utilized to verify the normality and homoscedasticity of the residuals, respectively. Multiple comparisons among different groups were conducted using Bonferroni's test. Data were subsequently analyzed using a linear regression model.

The X-ray diffraction (XRD) measurements revealed no significant differences in the lattice parameters, crystallite size, and lattice microdeformations among varying numbers of iterations. Statistical analysis was conducted utilizing Statgraphics XIX Centurion [15].

## 3. Results and discussion

This investigation aimed to ascertain the morphological and structural alterations of WOG instruments subjected to standard operation in a simulated experimental environment. J-shaped resin canals impose severe torsional load conditions, such as screw-in effects, on the endodontic instrument [16], [17]. The endodontic instruments underwent substantial deformations prior to fracture; the spiraling geometric configuration of the endodontic instrument generated an increase in the apical and coronal driving forces that untwisted the instrument from the tip and abraded the cutting edges [17], [18].

### 3.1. Optical microscopy

An initial set of ten random measurements was conducted between standard calibrated length elements to estimate the measurement error associated with the initial and final lengths of the machining paths. Subsequently, an additional set of ten random measurements was performed for variance comparison purposes. Utilizing the F-statistic, the variances of the two sets of measurements were determined to be equal with 99% confidence, yielding a p-value of 0.6445. Consequently, length measurements on images with a resolution of  $1280 \times 1024$  pixels were found to have an associated error of  $1.38 \mu\text{m}$ .

Figure 3 illustrates the surface geometrical variations at 100x magnification for the segment of interest in the WOG instrument (5 mm from the tip). Surface variations were observed for different numbers of pecks. Untwisting, unbending, and elongations were most pronounced at values approximating 54 pecks, and segment separation occurred at 62 pecks.

Bézier curve measurements were conducted on five WOG instrument images, and MATLAB® software was utilized to calculate the Cauchy strain using Equation 1.



The results indicated that the number of peaks significantly influenced the Lagrangian deformation. The p-value of the normality of the residuals approximated the type I error value ( $\alpha = 0.05$ ). Consequently, the ANOVA results with 95% confidence demonstrated a statistically significant difference with a p-value  $< 0.001$ . Table 1 presents an example of the strain measurements, specifically for 40, 52, 62, 76, and 80 pecks. The analysis of variance (ANOVA) shown in Table 2, revealed statistically significant differences in the Cauchy strain values among the three groups: 40 and 62 pecks, 62 and 76 pecks, and 62 and 80 pecks.

The maximum strain values were observed at failure at 62 pecks, with a magnitude of 12.5%. The strain values were lower for failure at 76 pecks (10.8%) and 80 pecks (9.2%). The subsequent constriction represents a narrowing of the endodontic instrument associated with a sudden ductile fracture, as illustrated in Figure 4(a). A predictive model correlating the number of pecks to the percentage of strain was developed using least-squares adjustment. The optimal fit was achieved with a fourth-order polynomial, demonstrating a correlation of 80.5%

at a 95% confidence level for the regressors. The derived model is presented in Equation 2.

$$\varepsilon_c = a_0 + a_1P + a_2P^2 + a_3P^3 + a_4P^4 \quad (2)$$

Where  $\varepsilon_c$ , is the percentage of Cauchy or Lagrangian strain,  $P$  is the number of pecks, and  $a_i$ ,  $i = 1, 2, 3, 4$  correspond to the linearly fitted regressors. In the specific experimental domain, WOG was employed on the canals with the motor's revolutions and torque as specified by the manufacturer, at an ambient temperature of  $38^\circ \pm 1^\circ\text{C}$ . The values of the regressors are presented in Table 3.

Table 3. Model regression coefficients

Regressor coefficient	Value
$a_0$	529.6
$a_1$	-38.31
$a_2$	1.012
$a_3$	-0.01141
$a_4$	0.4673(10 <sup>-6</sup> )

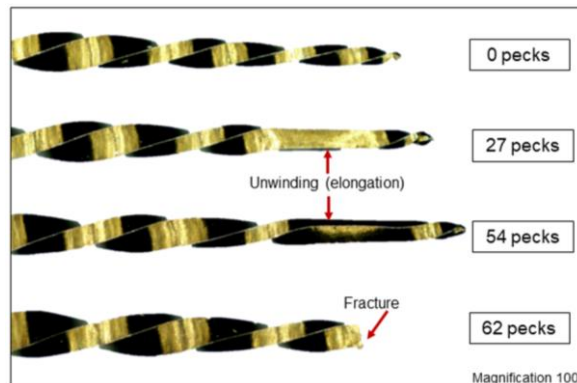


Figure 3. Optical microscopy of WOG Primary instrument used on different numbers of pecks.

Table 1. Strain measurements.

Number of pecks	Cauchy Strain measurement ( $\varepsilon_c$ ) [%]				
	1	2	3	4	5
40	4.571	7.423	4.087	3.911	4.303
52	7.985	10.140	9.314	6.853	7.932
62	9.671	12.290	10.290	13.760	17.180
76	4.940	6.765	7.778	6.690	8.832
80	7.450	6.239	5.519	5.194	6.875

Table 2. Analysis of variance

Source of variation	SS	df	MS	P-value	Fcrit
Between Groups	177.331	4	44.3328	0.0000	14.03
Within Groups	63.1847	20	3.1592		
Total	240.516	24			

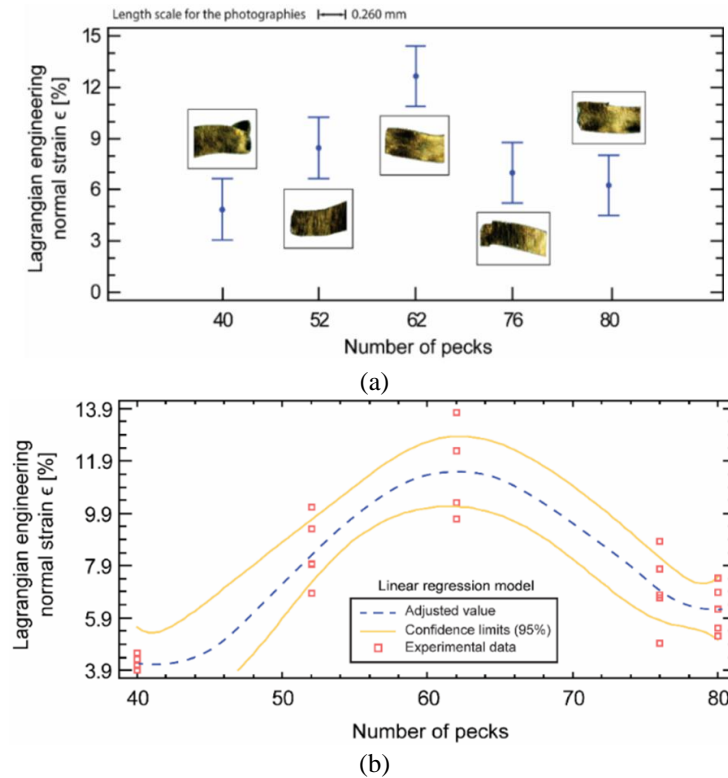


Figure 4. (a) Mean plot for Cauchy strains. (b) Polynomial fit.

This model predicts that the strain percentage increases with the number of pecks, reaching a maximum strain value ( $\approx 11\%$ ) at 62 pecks. After this point, the strain rate slightly decreased. A correlation of 80.5% indicates that the model is an excellent fit for the data. The confidence interval for the regressors indicates a 95% probability that the model accurately predicts the strain percentage for a given number of pecks.

Experimental findings indicated that resin canal instrumentation necessitated 16 pecks, equivalent to four radicular artificial canals. After 62 pecks, the strains began to decrease due to severe plastic deformation of the endodontic instrument prior to sudden fracture, as illustrated in Figure 4(b). The subsequent sudden fracture occurred as a result of excessive deformation caused by torsional loads in ductile failure [19], analogous to those reported in other research studies, namely for ProTaper, Hand Use, and K3 references [20]; for ProFile and ProTaper [21]; for EndoSequence and ProFile Vortex instruments [22]; for Typhoon CM instruments [23]; for Wave One Primary, ProTaper Next, Hyflex Cm, Hyflex EDM, and F6 SkyTaper [24]; and for JIZAI endodontic instruments, among others. However, none of these investigations proposed models that correlated endodontic instrument variations with the number of pecks.

### 3.2. Scanning electron microscopy

Figure 5(top) presents a longitudinal view of the fractured instrument obtained using scanning electron microscopy (SEM). In the area proximal to the fracture 5(a), the machining lines exhibit deformation, resulting in stretching; consequently, the elongation of the instrument is discernible and quantifiable in the optical microscopy images.

These deformations are associated with plastic strain, generating shear bands that cause separations in various instrument segments, as illustrated near the fracture in Fig. 5(b). Conversely, in the region distal to the fracture 5(c), it was observed that the machining lines maintain a "horizontal" orientation without apparent deformation.

The fracture is associated with the propagation of cracks, which experience accelerated expansion due to defects, phases, and geometric conditions. Figure 5(bottom) illustrates the cross-sectional view of the fracture. It is evident that microcracks 5(d), shear lips 5(e), abrasive marks indicative of ductile torsion, and 5(g) dimpled fibrous zones characteristic of overburden are present.

Scanning electron microscopy (SEM) images of the fractured surface revealed characteristic features of ductile torsional failure, including concentric abrasion

marks and fibrous dimple marks at the center of rotation [25], [26]. The evidence indicates that ductile torsional shear failure occurred. This failure mode is characterized by its manifestation along the same transverse plane of the instrument. The observed untangling and substantial plastic strains are associated with the ductile behavior of the NiTi alloy and torsional stress when the instrument tip becomes immobilized against the canal wall [27], [28]. The torsional load originated from the friction between the cutting flutes of the endodontic instrument and canal walls. While irrigation reduces this friction, the removed canal material acts as an abrasive, consequently increasing the friction and torsional load.

In this study, the frictional loads were elevated due to the canal material, friction coefficients, and wear effects

resulting from the adhesion of the endodontic instrument to the polymer [29]. Adhesion between the cutting edges and artificial canal walls creates a sensation for the endodontist that the instrument is being drawn into the canal in the apical direction. The clinician subsequently attempts to counteract this phenomenon, exerting force on the instrument in the outward direction, thereby accelerating the fracture of the endodontic tool.

Within the context of this study and considering the properties of the artificial canals fabricated from Diallyl Phthalate (Poly) and the resultant friction with the instrument, torsional forces exert a more substantial influence on fracture (including fatigue-induced fracture) despite the instrumentation of curved canals.

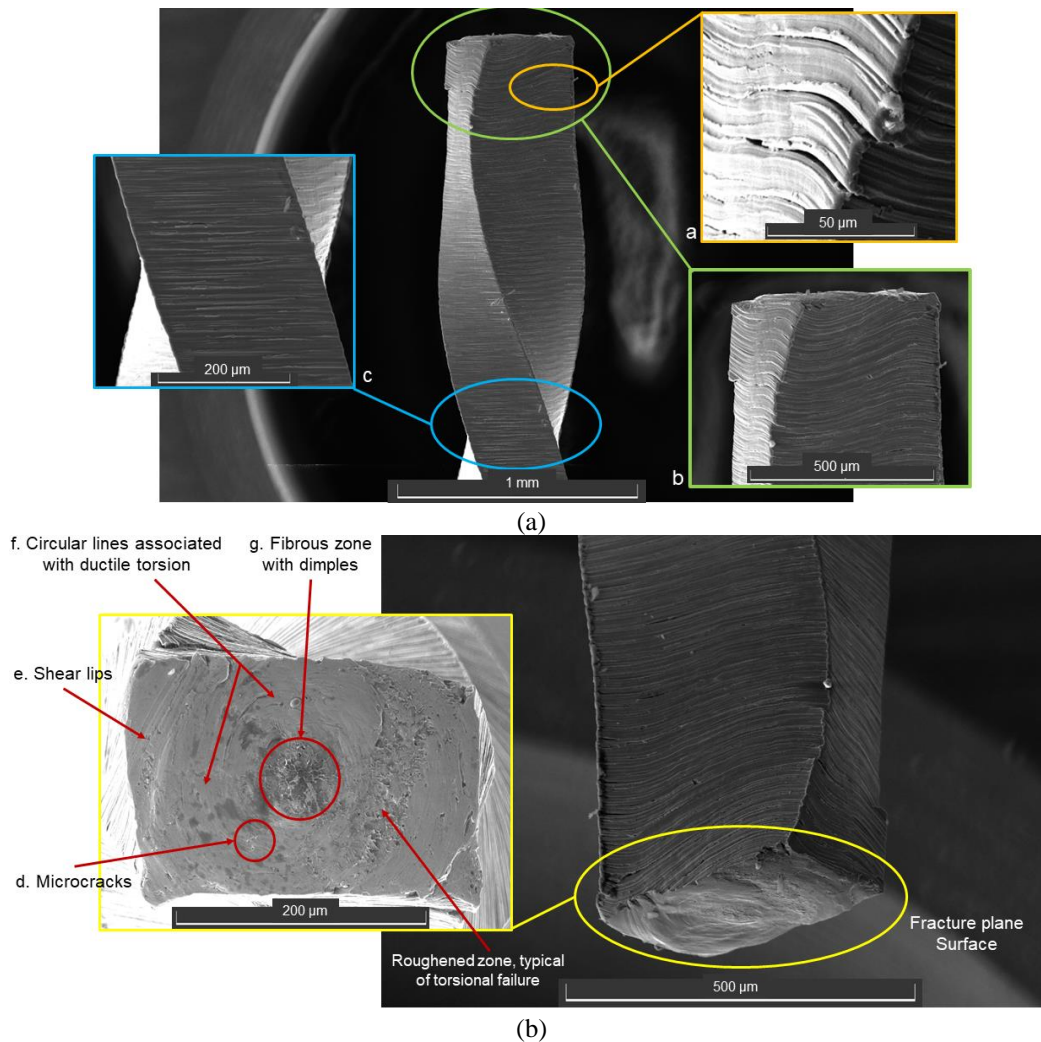


Figure 5. SEM images of WOG. Top: Longitudinal view, (a) section near the fracture, (b) shear band, (c) undeformed machining lines. Bottom: Cross-sectional view of the fracture plane: (d) microcracks, (e) shear lips, (f) concentric marks, (g) dimples.

### 3.3. X-ray diffraction

Figure 6(a) presents a wide  $2\theta$  range diffraction pattern of a NiTi endodontic instrument, in which three intensities were observed. The first intensity manifested as a broad peak corresponding to inelastic scattering from the sample holder and the optics setup. Due to the complex geometry of the specimen, modifications were implemented to the sample holder to align the zone of interest of the endodontic instrument tangentially to the focusing circle of the diffractometer.

Due to the small size of the WOG Primary, the X-ray beam interacted with the area of interest of the specimen and sample holder. The third intensity manifests as a sharp peak corresponding to the diffraction signal from the WOG instrument (highlighted in the diffraction pattern and shown in Figure 6(b)). The aperture slits of the divergent and antivergent X-ray beams were utilized to reduce the background noise without diminishing the intensity of the diffraction peaks. Four measurements were conducted with aperture values of 3 mm, 2 mm, 1 mm, and 0.7 mm. The diffraction signal improves as the aperture value decreases; consequently, the slits aperture was fixed at 0.7 mm for all subsequent measurements.

The diffraction patterns corresponding to the NiTi WOG instruments at the 0, 27, and 54 pecks are presented in Figure 6(c).

Through a systematic search procedure utilizing the AMCSD database [30], the  $(2\bar{1}2)$  and  $(300)$  planes of the R-phase of the NiTi alloy (AMCSD code 0018899) were identified to correspond to the diffraction peaks of the pattern, exhibiting a structure belonging to the trigonal symmetry group, which is consistent with previous reports for WOG Primary instruments, primarily composed of a martensite phase [31], [32].

The discrepancy between the relative intensities of  $(2\bar{1}2)$  and  $(300)$  indicates evidence of texture changes. This phenomenon has been previously documented, wherein NiTi R-phase grains reorient due to the deformation of the instrument during cycling when loads are applied [33], [34], resulting in both untwisting (axial deformation) and shear bands (longitudinal deformation). The texture variation observed at 27 pecks suggests that the variation is associated with grain reorientation induced by the application of load.

The microstructure of the instruments was investigated as a function of lattice parameters, crystallite size, and microstrains. The lattice parameters, crystalline size, and micro deformations were determined by refining the

diffraction pattern using GSAS [35] with the type 4 function of the software, while the texture coefficient was obtained from an analysis of relative intensities using the Harris equation. The intensities were extracted by fitting with a pseudo-Voigt function in Origin Pro [36].

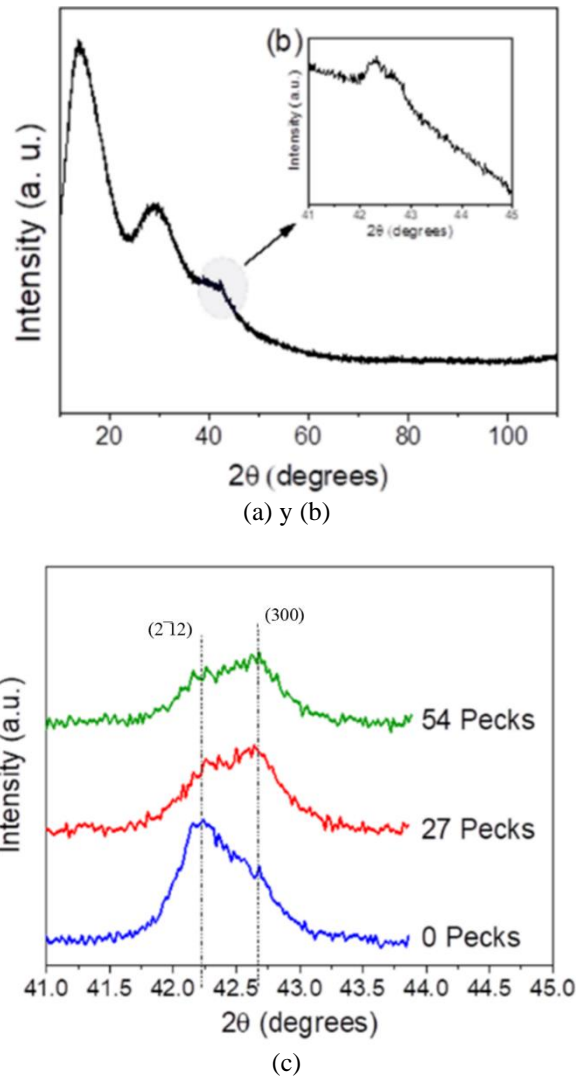


Figure 6. WOG Primary (a) Original diffraction pattern, (b) Diffraction signal, and (c) Diffraction patterns at 0, 27, and 54 pecks

The lattice parameters remained approximately constant, suggesting that the deformation processes did not result in variations of these parameters, as illustrated in Figure 7(a). Generally, a reduction in microstrain indicates the elimination of defects through recrystallization. This phenomenon typically implies an increase in crystallite size, a behavior that is not observed in this case, as demonstrated in Figure 7(b).



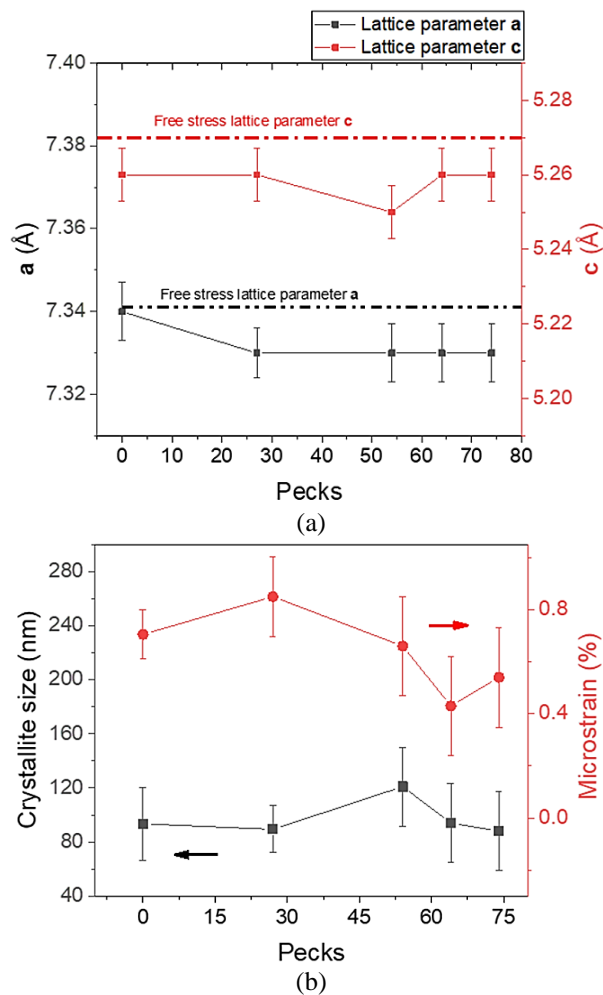


Figure 7. WOG Primary (a) Lattice parameters, and (b) Crystallite size and microstrains.

Crystallite size values for this material have been reported between 10 nm and 230 nm [37] and between 25 and 55 nm [38]. Some studies have reported microstrains between 17 and 32% [38]. These values are dependent on the method of NiTi production.

All samples generally exhibited compressive stress with respect to the free stress lattice parameter value, which can result from various factors, including machining heat treatment and coating processes. Compressive stress manifested when cycles were applied. Deformation occurred and, under the experimental conditions, no variations in higher lattice parameters (tensile stress) were observed, indicating that, despite the diverse load directions (longitudinal, torsional, and flexural) applied to the instrument, only minimal compression or constant stress was detected as a function of instrumentation (pecks).

From a structural perspective, the microstructure of the specimens was examined as a function of lattice defects through crystallite size and microstrain analyses. The crystallite size remained approximately constant for all endodontic instruments, suggesting that the deformation processes did not result in crystallite size variations, as illustrated in Figure 7(b).

The martensite R-phase texture exhibited a significant variation with the number of pecks (ANOVA 95%, p-value=0). To validate the normality assumption, a variable transformation was necessary for texture (Lilliefors test, p-value=0.6621). The optimal fit for the predictive model was achieved using the natural logarithm of the texture. The model is shown in Equation 3.

$$\ln(T) = a_0 + a_1P + a_2P^2 + a_3P^3 \quad (3)$$

Where  $T$  is the texture,  $P$  is the number of pecks, and  $a_i$ ,  $i = 0,1,2,3$  correspond to the regressors coefficients, whose values are shown in Table 3.

Table 3. Model regression coefficients for texture model

Regressor coefficient	Regressor value
$a_0$	0.239822
$a_1$	-0.033980
$a_2$	$0.18 \times 10^{-4}$
$a_3$	$-0.525 \times 10^{-6}$

In the new WOG Primary, the preferential plane is  $(2\bar{1}2)$ , and. As the number of pecks increased, the texture decreased significantly, indicating grain reorientation, which suggests a change in the preferential plane. After 40 pecks, the texture increased marginally. It reached a maximum value at 62 points, maintaining (300) as the preferential plane. After 62 pecks, there was another decrease in texture, indicating new grain reorientation associated with the most prominent strain of the endodontic instrument. The polynomial fit is shown in Figure 8.

Texture measurements were employed to ascertain the orientation of crystalline grains, and it was observed that the natural logarithm of the texture exhibited a correlation with the number of pecks. Texture modification was substantiated by the progression of the natural logarithm from negative to positive values.

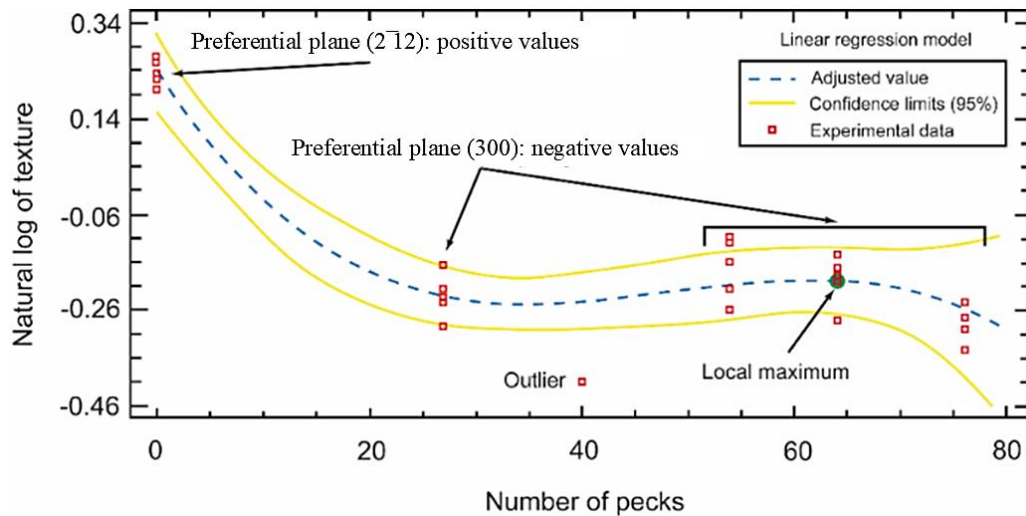


Figure 8. Regression plot for texture model.

Beyond 20 pecks, the natural texture logarithm demonstrated a slight increase until it attained a local maximum at 62 pecks, coinciding with the maximum strain level on the endodontic surface. A gradual process of grain reorientation occurred as the instrument underwent untangling (formation of shear bands). Subsequent to 62 pecks, a decrease in the value of the natural logarithm of texture was observed, indicating a new grain reorientation. The local minimum assumption suggests that grain reorientation between the 62 and 74 pecks occurs rapidly. Consequently, the formation of a shear band is hypothesized to be critical within this interval of pecks.

The diffraction signal represents an aggregate of contributions from a region exhibiting heterogeneity in deformation types. This phenomenon indicates that the phase transformations induced by deformations applied during cycles to the endodontic instrument are accompanied by certain stress relief mechanisms.

A slight reduction in the microstrain provides evidence of defect elimination through recrystallization. Additionally, the texture (grain reorientation) varied significantly with the number of pecks. Two preferential planes indicated the presence of twinned martensite variants:  $R(2\bar{1}2)$  for zero pecks and  $R(300)$  upon the initiation of instrumentation. Macroscopic changes can be attributed to the growth of martensitic grains at the expense of others and the motion of twin boundaries that alters their orientation [39]. Due to the instrument exhibiting untangling, a gradual process of grain reorientation was associated with the formation of shear bands. Subsequently, grain reorientation occurred rapidly between the 40 and 62 pecks, and the formation of shear bands was critical within these intervals.

Several studies have focused on characterizing endodontic instruments using XRD [40], [41], [42], [43]; however, there remains a significant gap in research related to the structural characterization of NiTi endodontic instruments for clinical use. This study demonstrated that the morphological and structural properties of endodontic instruments are influenced by their utilization, subsequently altering their performance.

#### 4. Conclusions

The surface characteristics of the WOG Primary instrument were investigated in a simulated environment for various cycles of use. The morphological evolution of the instrument surface was observed, the images were documented, and the strain was quantified. A correlation was established between the geometric alterations of the surface and the WOG operational parameters. After 12.5%, the endodontic instrument exhibited a reduction in thickness (elongation). Beyond this threshold, WOG undergoes significant elongation, which may potentially compromise the performance of the instrument and increase the likelihood of sudden fracture. Instrument failure occurred in approximately 62 pecks (equivalent to five artificial canals).

Plastic deformations were observed in the instrument and were attributed to a ductile failure mechanism caused by torsion-adhesion associated with the material of the artificial canal. Furthermore, the shear bands were correlated with the initiation of ductile failure, and plastic deformation was associated with the reorientation of the alloy grains. Subsequently, the number of pecks may correlate with endodontic instrument failure.

Mathematical models were proposed to predict the strain and texture variations as a function of the peck count. The application of Lagrangian methods and Cauchy strain measurements was validated through texture analysis, which structurally elucidated macroscopic strains. The polynomial fit can be utilized to predict the percentage of Lagrangian strain for any number of pecks within the range of the data employed in the model fitting. The change in the grain orientation of the alloy was corroborated between 0 and 20 pecks, and a subsequent change was observed after 62 pecks, which elucidates the occurrence of plastic deformation. However, it is imperative to note that the validity of the model is confined to a specific experimental domain.

This novel methodology involved subjecting an endodontic instrument to simulated endodontic treatment in a laboratory environment, quantifying the number of pecking motions until fracture occurred, and measuring the strain in a region proximal to the maximum bending zone (canal curvature) using optical microscopy. The scope of this study is limited to instruments in which the strains associated with the original machining paths of WOG instruments can be recorded. The process was validated through an XRD measurement of the texture, which provided a structural explanation for the observed macroscopic strains.

#### Funding and acknowledgments

The authors acknowledge the support provided by the Ministry of Science, Technology, and Innovation (MinCiencias) of the Republic of Colombia through grant 909 for the doctoral studies of Y.M. Orozco-Ocampo. The authors extend their appreciation to Vortex Company for facilitating SEM image acquisitions. Furthermore, the authors express their gratitude to Dr. Elizabeth Restrepo Parra and the team at LAFIP of the Universidad Nacional de Colombia, Campus Manizales, for conducting the XRD tests.

#### Autor Contributions

Y. M. Orozco-Ocampo: Data Curation, Formal Analysis, Investigation, Methodology, Validation, Writing of Original Draft, Writing-Review, Editing. C.A. Álvarez-Vargas: Conceptualization, Formal Analysis, Methodology, Validation, Writing of The Original Draft, Writing-Review, and Editing. F. N Jiménez-García: Methodology, Project Administration, Writing of Original Draft, Writing-Review, and Editing. D. Escobar-Rincón: Data Curation, Formal Analysis, Investigation, Methodology, and Writing of The Original Draft. P. X. Jaramillo-Gil: Investigation, Methodology.

#### Conflicts of Interest

The authors declare no conflict of interest.

#### Institutional Review Board Statement

Not applicable.

#### Informed Consent Statement

Not applicable.

#### References

- [1] G. R. M. La Rosa, F. S. Canova, L. Generali, E. Pedullà, “The Role of Pecking Motion Depths in Dynamic Cyclic Fatigue Resistance: In Vitro Study,” *Int Dent J*, vol. 1, pp. 1–7, Feb. 2024, doi: <https://doi.org/10.1016/j.identj.2024.01.014>
- [2] M. B. McGuigan, C. Louca, and H. F. Duncan, “Endodontic instrument fracture: Causes and prevention,” *Br Dent J*, vol. 214, no. 7, pp. 341–348, 2013, doi: <https://doi.org/10.1038/sj.bdj.2013.324>
- [3] A. Carvalho, M. Freitas, L. Reis, D. Montalvão, and M. Fonte, “Rotary Fatigue Testing to Determine the Fatigue Life of NiTi alloy Wires: An Experimental and Numerical Analysis,” *Procedia Structural Integrity*, vol. 1, pp. 34–41, 2016, doi: <https://doi.org/10.1016/j.prostr.2016.02.006>
- [4] M. J. Mahtabi, N. Shamsaei, and M. R. Mitchell, “Fatigue of Nitinol: The state-of-the-art and ongoing challenges,” *J Mech Behav Biomed Mater*, vol. 50, pp. 228–254, 2015, doi: <https://doi.org/10.1016/j.jmbbm.2015.06.010>
- [5] L. Testarelli et al., “Cyclic fatigue of NiTi instruments used in complex curvatures with continuous or reciprocating rotation,” *G Ital Endod*, vol. 28, no. 2, pp. 87–90, 2014, doi: <https://doi.org/10.1016/j.gien.2014.10.003>
- [6] N. E. Dowling, *Mechanical Behavior of Materials - Engineering Methods for Deformation, Fracture, and Fatigue*, Fourth., vol. Fourth Edition. 2013.
- [7] Y. M. Orozco-Ocampo, “Influencia de los parámetros de corte en el desgaste de micro-herramientas para micro-mecanizado de materiales biocompatibles,” Tesis de Maestría en Ingeniería Mecánica, Universidad del Norte, 2012.

- [8] H. P. Lopes, C. N. Elias, M. V. B. Vieira, V. T. L. Vieira, L. C. De Souza, A. L. Dos Santos, "Influence of Surface Roughness on the Fatigue Life of Nickel-Titanium Rotary Endodontic Instruments," *J Endod*, vol. 42, no. 6, pp. 965–968, 2016, doi: <https://doi.org/10.1016/j.joen.2016.03.001>
- [9] I. S. Kang, J. S. Kim, M. C. Kang, and K. Y. Lee, "Tool condition and machined surface monitoring for micro-lens array fabrication in mechanical machining," *J Mater Process Technol*, vol. 201, no. 1–3, pp. 585–589, May 2008, doi: <https://doi.org/10.1016/j.jmatprotec.2007.11.187>
- [10] P. R. Garcia, P. D. Resende, N. I. A. Lopes, I. F. da C. Peixoto, V. T. L. Buono, and A. C. D. Viana, "Structural Characteristics and Torsional Resistance Evaluation of WaveOne and WaveOne Gold Instruments after Simulated Clinical Use," *J Endod*, vol. 45, no. 8, pp. 1041–1046, 2019, doi: <https://doi.org/10.1016/j.joen.2019.04.009>
- [11] M. G. A. Bahia, M. C. C. Melo, and V. T. L. Buono, "Influence of simulated clinical use on the torsional behavior of nickel-titanium rotary endodontic instruments," *Oral Surgery, Oral Medicine, Oral Pathology, Oral Radiology and Endodontology*, vol. 101, no. 5, pp. 675–680, 2006, doi: <https://doi.org/10.1016/j.tripleo.2005.04.019>
- [12] D. Al-Sudani et al., "Cyclic fatigue of nickel-titanium rotary instruments in a double (S-shaped) simulated curvature," *J Endod*, vol. 38, no. 7, pp. 987–989, 2012, doi: <https://doi.org/10.1016/j.joen.2012.03.025>
- [13] P. Van der Vyver and M. Vorster, "Clinical application of WaveOne® Gold reciprocating instruments: part 1," *Endodontic Practice*, 2021. [Online]. Available: <https://endopracticeus.com/ce-articles/clinical-application-of-waveone-gold-reciprocating-instruments-part-1/>
- [14] C. A. Schneider, W. S. Rasband, and K. W. Eliceiri, "NIH Image to ImageJ: 25 years of image analysis," *Nat Methods*, vol. 9, no. 7, pp. 671–675, Jul. 2012, doi: <https://doi.org/10.1038/nmeth.2089>
- [15] I. Statgraphics Technologies, "Statgraphics Centurion XIX," *The Plains, Virginia*: 19.
- [16] J. H. Ha, S. W. Kwak, A. Sigurdsson, S. W. Chang, S. K. Kim, and H. C. Kim, "Stress Generation during Pecking Motion of Rotary Nickel-titanium Instruments with Different Pecking Depth," *J Endod*, vol. 43, no. 10, pp. 1688–1691, Oct. 2017, doi: <https://doi.org/10.1016/j.joen.2017.04.013>
- [17] J. H. Ha, S. S. Park, "Influence of glide path on the screw-in effect and torque of nickel-titanium rotary files in simulated resin root canals," *Restor Dent Endod*, vol. 37, no. 4, p. 215, 2012, doi: <https://doi.org/10.5395/rde.2012.37.4.215>
- [18] V. Faus-Llácer, N. H. Kharrat, C. Ruiz-Sánchez, I. Faus-Matoses, Á. Zubizarreta-Macho, and V. Faus-Matoses, "The effect of taper and apical diameter on the cyclic fatigue resistance of rotary endodontic files using an experimental electronic device," *Applied Sciences*, vol. 11, no. 2, pp. 1–14, 2021, doi: <https://doi.org/10.3390/app11020863>
- [19] Y. Shen, G. S. pan Cheung, B. Peng, and M. Haapasalo, "Defects in Nickel-Titanium Instruments after Clinical Use. Part 2: Fractographic Analysis of Fractured Surface in a Cohort Study," *J Endod*, vol. 35, no. 1, 2009, doi: <https://doi.org/10.1016/j.joen.2008.10.013>
- [20] J. Y. Kim, G. Shun-Pan Cheung, S. H. Park, D. C. Ko, J. W. Kim, H. C. Kim, "Effect from cyclic fatigue of nickel-titanium rotary files on torsional resistance," *J Endod*, vol. 38, no. 4, pp. 527–530, Apr. 2012, doi: <https://doi.org/10.1016/j.joen.2011.12.018>
- [21] R. C. Wycoff and D. W. Berzins, "An in vitro comparison of torsional stress properties of three different rotary nickel-titanium files with a similar cross-sectional design," *J Endod*, vol. 38, no. 8, pp. 1118–1120, Aug. 2012, doi: <https://doi.org/10.1016/j.joen.2012.04.022>
- [22] L. Campbell, Y. Shen, H. M. Zhou, M. Haapasalo, "Effect of fatigue on torsional failure of nickel-titanium controlled memory instruments," *J Endod*, vol. 40, no. 4, 2014, doi: <https://doi.org/10.1016/j.joen.2013.12.035>
- [23] F. Lo Savio, E. Pedullà, E. Rapisarda, G. La Rosa, "Influence of heat-treatment on torsional resistance to fracture of nickel-titanium endodontic instruments," in *Procedia Structural Integrity*, 2016. doi: <https://doi.org/10.1016/j.prostr.2016.06.167>
- [24] M. Thu et al., "Influence of different kinematics on stationary and dynamic torsional behavior of JIZAI nickel-titanium rotary instruments: An in vitro study," *J Dent Sci*, vol. 18, no. 3, 2023, doi: <https://doi.org/10.1016/j.jds.2022.10.005>
- [25] F. Lo Savio, E. Pedullà, E. Rapisarda, and G. La Rosa, "Influence of heat-treatment on torsional resistance to fracture of nickel-titanium endodontic instruments," *Procedia Structural Integrity*, vol. 2, pp. 1311–1318, 2016, doi: <https://doi.org/10.1016/j.prostr.2016.06.167>



- [26] L. Campbell, Y. Shen, H. M. Zhou, and M. Haapasalo, "Effect of fatigue on torsional failure of nickel-titanium controlled memory instruments," *J Endod*, vol. 40, no. 4, pp. 562–565, 2014, doi: <https://doi.org/10.1016/j.joen.2013.12.035>
- [27] R. C. Wycoff, D. W. Berzins, "An In Vitro Comparison of Torsional Stress Properties of Three Different Rotary Nickel-Titanium Files with a Similar Cross-Sectional Design," *J Endod*, vol. 38, no. 8, pp. 1118–1120, Aug. 2012, doi: <https://doi.org/10.1016/j.joen.2012.04.022>
- [28] J.-Y. Kim, G. Shun-Pan Cheung, S.-H. Park, D.-C. Ko, J.-W. Kim, and H.-C. Kim, "Effect from Cyclic Fatigue of Nickel-Titanium Rotary Files on Torsional Resistance," *J Endod*, vol. 38, no. 4, pp. 527–530, Apr. 2012, doi: <https://doi.org/10.1016/j.joen.2011.12.018>
- [29] M. Kucher, M. Dannemann, R. Füßel, M.-T. Weber, and N. Modler, "Sliding friction and wear of human teeth against biocompatible polyether ether ketone (PEEK) under various wear conditions," *Wear*, vol. 486–487, p. 204110, Dec. 2021, doi: <https://doi.org/10.1016/j.wear.2021.204110>
- [30] R. T. Downs and M. Hall-Wallace, "The American Mineralogist crystal structure database," *American Mineralogist*, vol. 88, pp. 247–250, 2003, 2023.
- [31] S. Oh et al., "Bending resistance and cyclic fatigue resistance of WaveOne Gold, Reciproc Blue, and HyFlex EDM instruments," *J Dent Sci*, vol. 15, no. 4, pp. 472–478, Dec. 2020, doi: <https://doi.org/10.1016/j.jds.2019.10.003>
- [32] M. Alcalde et al., "Cyclic fatigue and torsional strength of three different thermally treated reciprocating nickel-titanium instruments," *Clin Oral Investig*, vol. 22, May 2018, doi: <https://doi.org/10.1007/s00784-017-2295-8>
- [33] J. D. Ospina-Correa, D. A. Olaya-Muñoz, J. J. Toro-Castrillón, A. Toro, A. Ramírez-Hernández, and J. P. Hernández-Ortíz, "Grain polydispersity and coherent crystal reorientations are features to foster stress hotspots in polycrystalline alloys under load," *Science Advances*, vol. 7, no. 15, 2021, doi: <https://doi.org/10.1126/sciadv.abe3890>
- [34] M. Carl, B. Zhang, M. Young, "Texture and Strain Measurements from Bending of NiTi Shape Memory Alloy Wires," *Shape Memory and Superelasticity*, Jul. 2016, doi: <https://doi.org/10.1007/s40830-016-0073-0>
- [35] B. H. Toby and R. B. Von Dreele, "GSAS-II: The genesis of a modern open-source all purpose crystallography software package," *J Appl Crystallogr*, vol. 46, no. 2, pp. 544–549, Apr. 2013, doi: <https://doi.org/10.1107/S0021889813003531>
- [36] OriginLab Corporation, "Origin(Pro)," 2021, Northampton, MA, USA: 2021.
- [37] K. Huang, H. Yin, M. Li, Q. Sun, "Grain size dependence of stress-assisted two-way memory effect in Ti-50.04 at.% Ni shape memory alloy," *Materials Science and Engineering: A*, vol. 856, p. 143872, Oct. 2022, doi: <https://doi.org/10.1016/J.MSEA.2022.143872>
- [38] C. Jia, M. R. Akbarpour, M. Ahmadi Gharamaleki, T. Ebadzadeh, and H. S. Kim, "Synthesis and characterization of novel NiTi–Ni3Ti/SiC nanocomposites prepared by mechanical alloying and microwave-assisted sintering process," *Ceram Int*, vol. 49, no. 14, pp. 23358–23366, 2023, doi: <https://doi.org/10.1016/J.CERAMINT.2023.04.168>
- [39] M. R. Daymond, M. L. Young, J. D. Almer, D. C. Dunand, "Strain and texture evolution during mechanical loading of a crack tip in martensitic shape-memory NiTi," *Acta Mater*, vol. 55, no. 11, 2007, doi: <https://doi.org/10.1016/j.actamat.2007.03.013>
- [40] S. B. Alapati et al., "Metallurgical characterization of a new nickel-titanium wire for rotary endodontic instruments.," *J Endod*, vol. 35, no. 11, pp. 1589–1593, Nov. 2009, doi: <https://doi.org/10.1016/j.joen.2009.08.004>
- [41] G. Kuhn, L. Jordan, "Fatigue and mechanical properties of nickel-titanium endodontic instruments," *J Endod*, vol. 28, no. 10, pp. 716–720, 2002, doi: <https://doi.org/10.1097/00004770-200210000-00009>
- [42] L. Jordan, A. Sultan, and P. Vermaut, "Microstructural and mechanical characterizations of new NiTi endodontic instruments," *MATEC Web of Conferences*, vol. 33, 2015, doi: <https://doi.org/10.1051/mateconf/20153303005>
- [43] S. Zinelis, M. Darabara, T. Takase, K. Ogane, G. D. Papadimitriou, "The effect of thermal treatment on the resistance of nickel-titanium rotary files in cyclic fatigue," *Oral Surgery, Oral Medicine, Oral Pathology, Oral Radiology and Endodontology*, vol. 103, no. 6, pp. 843–847, 2007, doi: <https://doi.org/10.1016/j.tripleo.2006.12.026>